Dalton Transactions

Multi-metal coordination polymers grown through hybrid molecular layer deposition

Journal:	*Dalton Transactions*
Manuscript ID	DT-ART-02-2021-000465.R1
Article Type:	Paper
Date Submitted by the Author:	26-Feb-2021
Complete List of Authors:	Richey, Nathaniel; Stanford University, Department of Chemical Engineering Borhan, Shirin; Stanford University, Department of Chemical Engineering Bent, Stacey; Stanford University, Department of Chemical Engineering

Multi-metal coordination polymers grown through hybrid molecular layer deposition

Nathaniel E. Richey, Shirin Borhan, Stacey F. Bent*

*Email: sbent@stanford.edu

Department of Chemical Engineering, Stanford University, Stanford, CA, USA 94305

Abstract

Coordination polymers deposited by hybrid molecular layer deposition (MLD) techniques are of interest as highly conformal, functional materials. Addition of a second metal into these coordination polymers can result in additional functionality or fine tuning of the materials properties. Here, we investigate the deposition of multi-metal coordination polymers using hybrid MLD of Zn-Al and Zn-Hf with ethylene glycol as the organic linker. It is found that facile transmetalation occurs for the Zn-Al films, which results in Al-rich films, but does not take place for the Zn-Hf films. Additionally, the Zn-Hf films are found to be more resilient to ambient conditions than the pure Zn-based coordination polymer.

Introduction

Coordination polymers are a widely useful category of materials in which metal atoms are repeatedly connected through a bifunctional linker moiety.[1] Several subcategories of coordination polymers are well known and include examples such as metal organic frameworks,[2,3] Prussian blue analogues,[4] and metalcones.[5,6] *Metalcone* (e.g. alucone,[7] zincone,[8,9] or hafnicone[10]) is the colloquial name given to coordination polymers that are deposited through hybrid molecular layer deposition (MLD). Hybrid MLD is a technique that uses repeated, self-limiting surface reactions of organometallic and organic precursors to grow a desired metalcone film.[5,6] These metalcone films have been found to be suitable for a variety of applications such as molecule capture/release,[11] electrocatalysis,[12] energy storage,[13,14] and bioactive films.[15]

While many different metalcone films have been deposited, there are very few reports of metalcone films that contain more than one different metal.[16,17] Films of these more complex materials are of general interest, as they can allow for tuning of film properties based on the

ratios of the different metals within the film.[18,19] Atomic layer deposition (ALD), the inorganic equivalent of MLD, has long been used to deposit ternary and quaternary materials with two or three different metal centers present.[20,21] In fact, there have been over 250 unique ternary and quaternary ALD systems reported which include a wide variety of different combinations of metals, metalloids, and non-metals.[20] Yet, when two binary ALD processes are mixed to deposit a ternary film, it is not uncommon for deviations from the expected growth rate or composition to occur. These deviations mostly arise from switching between the two binary processes, since ALD (and MLD) are extremely surface sensitive and one binary process will result in formation of a different surface than the other. This repeated switching of the surface from one process to the other can result in lower-than-expected growth rates through active site poisoning from ligand exchange or incomplete ligand removal,[22,23] or even etching of the previous binary process.[24,25] Conversely, some ternary processes result in an increase in growth rate if one of the binary surfaces enhances nucleation of the other.[26] Not surprisingly, these deviations in growth rates will often also cause departures from the expected elemental composition of the final deposited film.

Hybrid MLD films provide a unique challenge over their ALD counterparts because the flexibility provided by the organic ligands could allow for diffusion of precursors into the film and even more pronounced effects from the interactions of the two metal centers. However, this effect has not been previously studied so the extent of such interactions is not yet known. Herein, we investigate the deposition of two multi-metal coordination polymers, Zn-Al and Zn-Hf with ethylene glycol. We show that the etching of Zn from the Al precursor is much more severe in the hybrid MLD process than it is from the pure ALD process, resulting in deposits that are significantly Al rich and Zn poor. Meanwhile, no etching is observed in Zn-Hf hybrid films and the atomic composition is linear with the binary cycle ratios. It is also observed that the presence of Hf helps to increase the ambient stability of the films when compared to pure zincone films.

Results and Discussion

In this study, we investigate the deposition of Zn-Al and Zn-Hf coordination polymers with ethylene glycol (EG) as the organic linker. Trimethylaluminum (TMA), diethylzinc (DEZ), and tetrakis(dimethylamido)hafnium (TDMAHf) were used as the Al, Zn, and Hf precursors,

respectively. These films were deposited using a *supercycle* approach, in which the binary hybrid MLD processes are combined in different ratios to deposit films with different compositions.[20] The supercycle recipe for these films takes the generic form of

$$n[x(DEZ - EG) - y((TMA\ or\ TDMAHf) - EG)]$$

where n is the number of supercycles, x is the number of the binary zincone cycles, and y is the number of the binary alucone or hafnicone cycles. Throughout this work, we will refer to films by their Zn cycle ratios as $\frac{x}{x+y}Zn$, or by a shorthand cycle number notation, $xZn{:}y(Al \text{ or } Hf)$ (i.e., a film where *x* = 4 and *y* = 1 will be referred to as either 0.8 Zn or 4Zn:1Al or 4Zn:1Hf). Unless otherwise noted, depositions were performed at 80 total cycles ($n(x+y) = 80$). More information about the experimental conditions can be found within the ESI.

We first studied the deposition of Zn-Al hybrid films as a coordination polymer equivalent of aluminum-doped zinc oxide (AZO). It has been shown in the literature that during the ALD of AZO, TMA can transmetalate with surface bound zinc species, forming volatile dimethylzinc which desorbs from the film.[25,27] This effect causes the Zn content in the AZO film to be as much as ~20% lower than expected when the ZnO cycle ratio is less than 90% of the total ALD cycles.[25] We observed a similar, yet much more pronounced, effect during the deposition of the Zn-Al hybrid films by MLD. Even at a zincone cycle ratio of 0.8 Zn, X-ray photoelectron spectroscopy (XPS) results show that less than 10% of the metal content in the film is Zn (Figure 1a, Figure S1). At the highest cycle ratio we investigated (79Zn:1Al), only 55% of the final metal content was zinc. We hypothesize that this significant increase in the transmetalation of zinc for aluminum in the hybrid films compared to the already-high propensity in the AZO system is due to the more flexible nature of the hybrid films, allowing the TMA to diffuse into the films and react with a larger percentage of the zinc species throughout the film (Figure 1b). The diffusion of TMA into the hybrid film is unsurprising, as it has been shown that TMA can diffuse deep into polymeric films during vapor phase infiltration experiments.[28] The substitution of Zn for Al has also been found to occur with several other Al precursors, such as aluminum chloride and aluminum isopropoxide, during the ALD of AZO.[29] Thus, while changing the steric bulk of the Al precursor

may decrease its diffusivity into the film, since Al appears to transmetalate with Zn regardless of the identity of the precursor ligand, we predict that Zn-Al hybrids would result in Zn-deficient films from similar transmetalation processes, regardless of the Al precursor used.

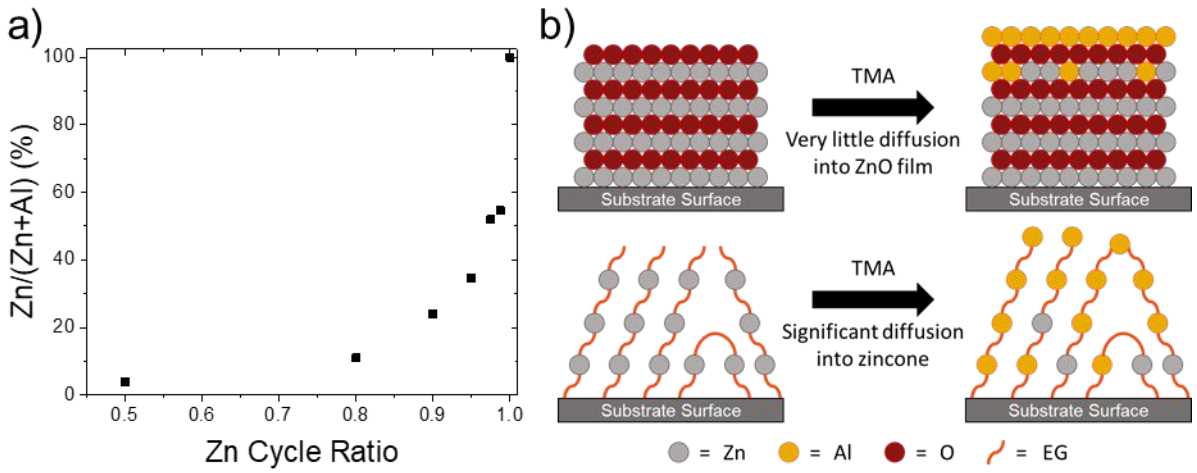

Figure 1. a) Estimated mole fraction of Zn calculated by XPS in [*x*Zn:*y*Al]-EG films grown at different cycle ratios. b) Representation of the interaction of TMA with a ZnO film (top) versus a zincone film (bottom), highlighting the increased transmetalation of TMA in zincone.

We next investigated Zn-Hf hybrid films. Hafnicone was chosen as the secondary MLD process because it has been grown previously and shown to be stable in air for several days.[10] Such stability is relatively unique among the metalcone films and we postulated that it might provide increased stability to the multi-metalcone hybrid films. Growth of Zn-Hf hybrid films was performed using DEZ, TDMAHf, and EG as precursors. Unlike the Zn-Al films, the deposited Zn-Hf hybrid films had a composition, as determined by XPS (Figure 2a), that was near linear with the zincone cycle ratio. The Zn fraction was further fitted using the "rule of mixtures" method, which assumes that the growth of zincone and hafnicone are independent of each other and so the composition is determined only by growth per cycle (GPC) and binary densities, as described in detail elsewhere.[25,26] The rule of mixtures fit was estimated by using measured GPC values of 0.9 and 1.4 Å/cycle along with previously reported densities of 1.9 and 3.0 g/cm^3 for zincone and hafnicone, respectively.[30] As evident in Figure 2a, the calculated rule of mixtures curve for Zn fraction deviates only slightly from linearity and fits the measured values very well, which indicates either that transmetalation does not occur between TDMAHf and the Zn species within

the film or that the byproduct of the transmetalation is not volatile and so remains in the film. We can rule out the retention of any transmetalation products in the film for the following reason. The byproduct of transmetalation would be a (dimethylamido)zinc species and, if these were trapped within the film, nitrogen would be observed by XPS. However, no nitrogen was detected (Figure S2), which likely precludes transmetalation chemistry. Hence, the result implies that transmetalation does not occur between TDMAHf and the Zn species. While the reason that the reaction does not occur for TDMAHf is not fully understood, the apparent lack of a secondary reaction between these two binary processes makes the deposition of the Zn-Hf hybrid films an excellent model to study. Growth per cycle of the Zn-Hf hybrid films also followed expected "rule of mixtures" like behavior (Figure 2b). Pure hafnicone films showed a growth per cycle of ~1.4 Å/cycle while zincone films grew at ~0.9 Å/cycle, both of which agree closely with previous reports,[8,10] and GPC followed the estimated rule of mixtures as Zn cycle ratio was changed.

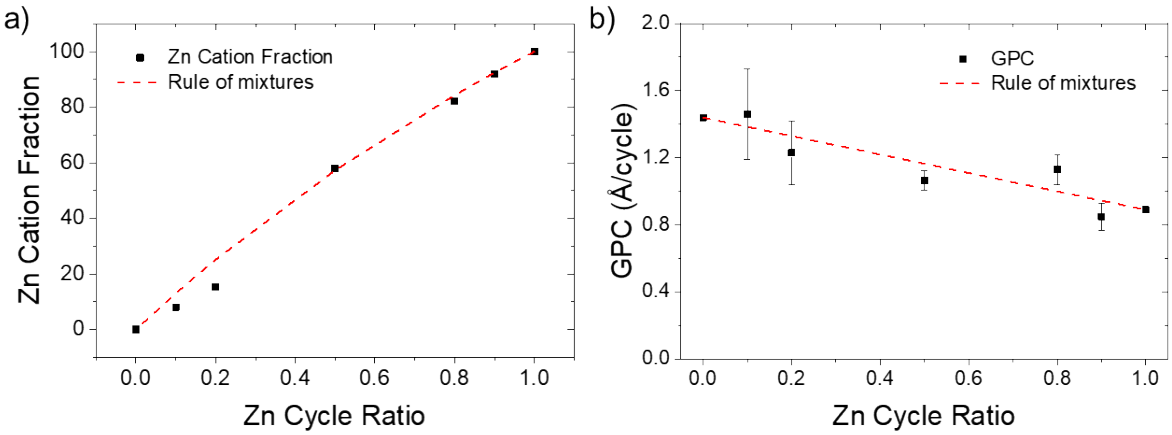

Figure 2. a) Estimated mole fraction of Zn calculated by XPS in [*x*Zn:*y*Hf]-EG films grown at different cycle ratios with a calculated rule of mixtures fit. b) Average GPC of Zn-Hf hybrid film with varying the Zn cycle ratio, also shown with calculated rule of mixtures fit. Error bars in (b) represent one standard deviation.

We used Fourier transform infrared (FTIR) spectroscopy to further characterize the nature of the deposited Zn-Hf hybrid films. From FTIR spectroscopy, we confirm that the EG linker is incorporated into the film through detection of the characteristic C-H stretches at ca. 2850 and 2930 and the C-O stretch at ca. 1095 cm^{-1} (Figure S3).[8,9] There are no significant differences in the position of these peaks in the FTIR spectrum across the different Zn-Hf ratios tested, including

the pure zincone and pure hafnicone films. This absence of a peak shift is not unexpected as the major peaks observed in the FTIR spectra arise from the EG linker and the wavenumbers of the EG-based modes should be largely independent of the metal center. Along with these expected peaks, a broad beak at approximately 3400 cm^{-1} is noted which is attributed to O-H stretching from the uptake of water into these films as they were exposed to ambient post deposition. This broad peak tends to be more pronounced in the more Zn-rich films and could be a result of the undercoordinated, divalent Zn centers within the films acting as a coordination site for water.

We also investigated the ambient stability of the mixed metal 1Zn:1Hf hybrid film in comparison to that of the pure zincone and hafnicone films. The 1Zn:1Hf mixture was selected for this study since it provides the greatest compositional differences from the two binary hybrid films. Previous reports on the ambient stability of zincone offer conflicting information: Byunghoon et al.[9] described very stable zincone films while Peng et al.[8] observed zincone films that degraded within an hour of exposure to humid air. Zincone films deposited by us showed behaviors similar to that reported by Peng et al. and rapidly degraded in ambient; in some cases, films degraded before an FTIR spectrum could be obtained (<10 min. after removal from reactor) (Figure S4). Hafnicone, on the other hand, was found to be relatively stable over 24 hours in ambient, with minimal decrease of the features related to the C-H and C-O stretches at 2850-2930 and 1095 cm^{-1}, respectively, similar to what was observed by Lee et al Figure S5).[10] Correspondingly, the 1Zn:1Hf hybrid film was found to be significantly more stable to ambient than pure zincone films. Results of FTIR spectroscopy studies of the 1Zn:1Hf films as a function of time in ambient are shown in Figure 3. A decrease in the C-H and C-O peak intensities from the 1Zn:1Hf films is evident within the first hour of exposure, but these modes do not disappear entirely even after 3 days in ambient. The decrease of the C-H and C-O peaks is accompanied by growth of peaks in the region between 1400-1700 cm^{-1}. Modes in this spectral region are associated with carboxylate groups. Hence, the growth of these peaks suggests the formation of carboxylate moieties within the film due to the oxidation of the alkoxides of the ethylene glycol linker.[12]

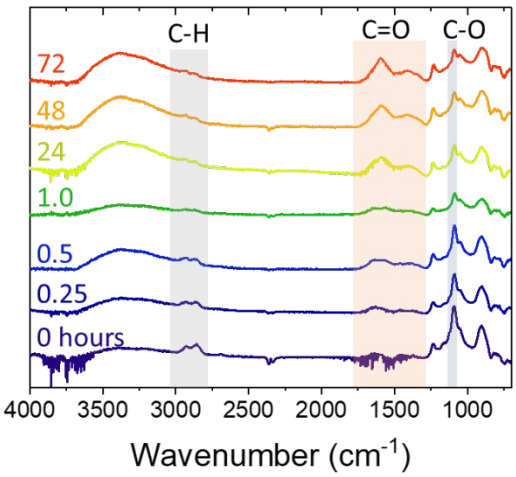

Figure 3. FTIR spectra of a 1Zn:1Hf hybrid film as a function of time in hours, over a period of 72 hours. Peaks corresponding to C-H and C-O stretches are highlighted.

High resolution XPS studies were also carried out on the 1Zn:1Hf hybrid films before and after three days of exposure to ambient and XPS peaks were assigned based on reported values from the NIST XPS database.[31] As seen in Figure 4, the O, Zn, and Hf XPS spectra change very little upon ambient exposure whereas the C 1s peak is shifted by 1.1 eV to lower binding energies, indicative of reduction of the C within the film. The C 1s spectra can be fitted into three component peaks at 284.6, 286.0, and 288.6 eV (Figure S6). The largest C 1s peak of the as-deposited film is centered at 286.0 eV and is attributed to the C-O within the EG linker. This peak decreases significantly after the 3 days of exposure to ambient. On the other hand, the peak at 284.6 eV, which is assigned to reduced carbon species that contain only C-C and C-H bonds, grows in size relative to the peak at 286.0 eV after air exposure. The decrease of the peak at 286.0 eV together with the increase of the peak at 284.6 eV likely indicates the breaking of the C-O bonds within the EG linker and the formation of new C-C or C-H bonds. Considering the lack of C-H peaks in the FTIR spectra after 3 days of exposure, we attribute the growth of the 284.6 eV XPS peak primarily to new C-C bonds, although a simple buildup of adventitious carbon could not be ruled out. We speculate that the presence of the 284.6 eV peak even in the as-deposited film could come from partial decomposition of the film prior to XPS or from adventitious C since, to avoid decomposition from ion bombardment, the films are not sputtered. Lastly, the small peak at 288.6 that forms after air exposure is attributed to oxidized C, likely in the form of carboxylate

moieties from oxidation of the EG linker, which corresponds well with what is observed in the FTIR spectra of the films after 3 days of air exposure.

We now return to the Hf, Zn and O XPS spectra. The unchanged Hf 4f XPS peaks, which are comprised of Hf $4f_{7/2}$ and $4f_{5/2}$, likely indicate that the oxidation state and the coordination of O around the Hf centers is very similar before and after exposure of the film to ambient. We note that because the Zn $2p_{3/2}$ peak does not change significantly with oxidation state, it was used as an internal reference set to 1022 eV and so no direct conclusions from the Zn 2p peak positions can be drawn.[31] However, the relatively high reduction potential for Zn^{2+} of 0.76 V and the oxidative environment of ambient make it unlikely that the Zn^{2+} center would have reduced during the decomposition of the film in ambient. The O 1s peak, which does not change significantly between 0 and 3 days, can be deconvoluted into two peaks at 531.7 and 530.4 eV (Figure S5). The peak at 530.4 eV matches well with previous reports of O within ZnO and HfO_2 and may indicate some cleavage of the C-O bond within the EG during or shortly after deposition.[32,33] The peak at 531.7 eV likely comes from oxygen in EG that is coordinating to both a carbon and a metal center. However, this peak could also be ascribed to metal-hydroxyl groups that may make up a portion of this peak after exposure to ambient, as the M-O-C bonding motifs could hydrolyze into M-O-H groups.[34] Our observations from FTIR spectroscopy and XPS are consistent with that observed by Bergsman et al. for EG-based manganicone films in ambient and likely indicate a similar final structure to what they proposed for manganicone after exposure to ambient air.[12] That final structure is a film in which the EG-linked hybrid partially decomposes to a mixture of metal oxide/hydroxide, adventitious carbon, and partially oxidized carboxylate linkers, with a small amount of non-decomposed hybrid film remaining.

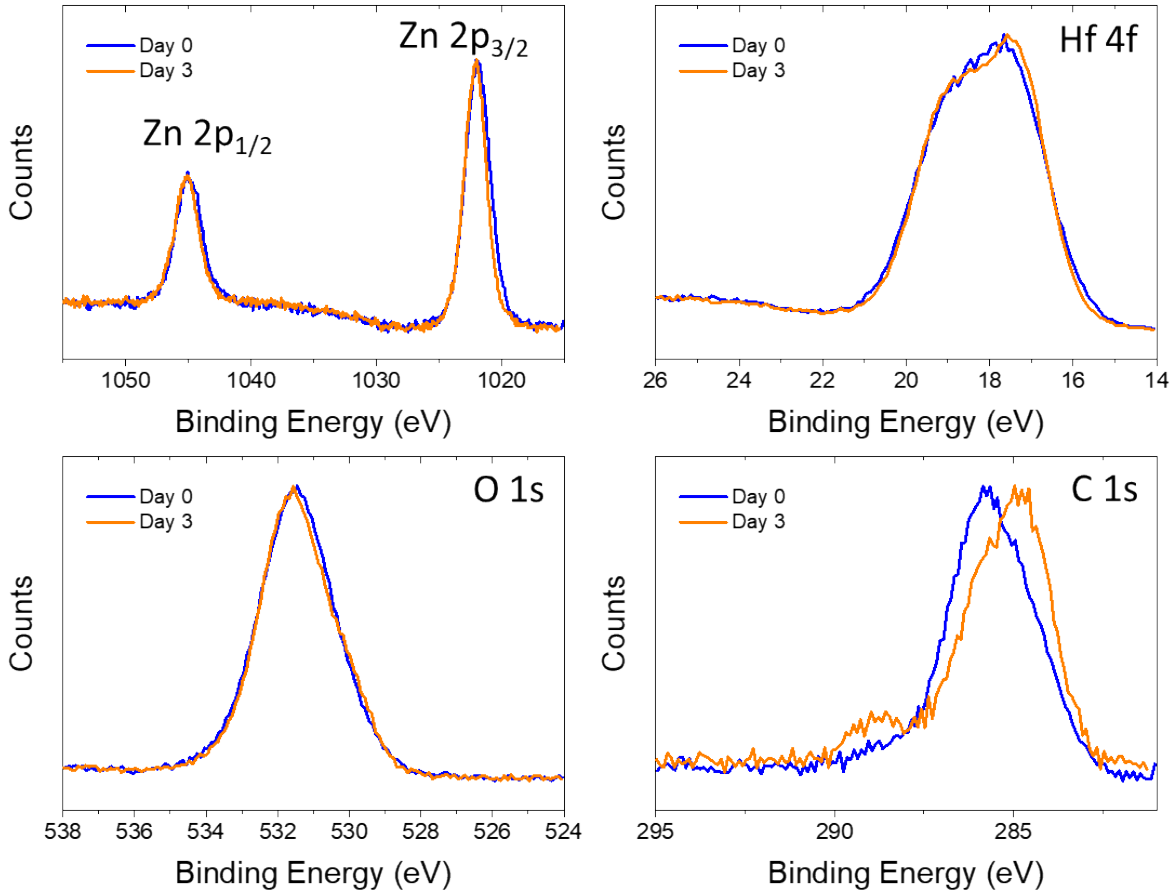

Figure 4. Normalized, high-resolution XPS scans of a 1Zn:1Hf hybrid film before and after three days of exposure to ambient.

Conclusions

We have shown that hybrid MLD can be used to deposit multi-metal coordination polymers with variable ratios of the different metals. Similar to what has been observed in the ALD of ternary metal oxides, these hybrid films can exhibit complex growth behaviors when certain combinations of precursors are used. In the deposition of Zn-Al hybrids, the transmetalation between TMA and already-deposited zinc species appears to proceed to a much higher degree than that observed during the ALD of AZO, an effect which we ascribe to the more flexible and porous nature of the hybrid films. Due to the prevalence of the transmetalation chemistry in this system, Zn-Al ratios are difficult to control and the resulting films are significantly more Al-rich than predicted. On the other hand, when TDMAHf is used in place of

TMA, the MLD process results in Zn-Hf hybrid films with a deposited Zn at. % that is nearly linear with the Zn cycle ratio used. These Zn-Hf hybrids were found to have greater air stability than zincone itself, which likely comes from the Hf within the film.

SUPPLEMENTAL INFORMATION

Supplemental information, including a description of the experimental methods, XPS and FTIR spectra of Zn-Al and Zn-Hf hybrid films as a function of Zn cycle ratio, FTIR spectra of zincone and hafnicone films as a function of ambient exposure, and high resolution XPS of Zn-Hf hybrid film upon exposure to ambient, can be found online at

ACKNOWLEDGEMENTS

We gratefully acknowledge Marie Krysak for helpful input and discussion. This work was supported by Intel SRS funding. Part of this work was performed at the Stanford Nano Shared Facilities (SNSF), supported by the National Science Foundation under award ECCS-2026822. We would also like to thank Camila de Paula for insights and discussion.

References

1 S. Kitagawa, R. Kitaura and S. Noro, *Angew. Chemie Int. Ed.*, 2004, **43**, 2334–2375.

2 O. K. Farha and J. T. Hupp, *Acc. Chem. Res.*, 2010, **43**, 1166–1175.

3 Q. L. Zhu and Q. Xu, *Chem. Soc. Rev.*, 2014, 43, 5468–5512.

4 W. J. Li, C. Han, G. Cheng, S. L. Chou, H. K. Liu and S. X. Dou, *Small*, 2019, 15, 1900470.

5 X. Meng, *J. Mater. Chem. A*, 2017, 5, 18326–18378.

6 P. Sundberg and M. Karppinen, *Beilstein J. Nanotechnol.*, 2014, 5, 1104–1136.

7 A. A. Dameron, D. Seghete, B. B. Burton, S. D. Davidson, A. S. Cavanagh, J. A. Bertrand and S. M. George, *Chem. Mater.*, 2008, **20**, 3315–3326.

8 Q. Peng, B. Gong, R. M. VanGundy and G. N. Parsons, *Chem. Mater.*, 2009, **21**, 820–830.

9 B. Yoon, J. L. O'Patchen, D. Seghete, A. S. Cavanagh and S. M. George, *Chem. Vap. Depos.*, 2009, **15**, 112–121.

10 B. H. Lee, V. R. Anderson and S. M. George, *ACS Appl. Mater. Interfaces*, 2014, **6**, 16880–16887.

11 A. Khayyami, A. Philip and M. Karppinen, *Angew. Chemie Int. Ed.*, 2019, **58**, 13400–13404.

12 D. S. Bergsman, J. G. Baker, R. G. Closser, C. MacIsaac, M. Lillethorup, A. L. Strickler, L. Azarnouche, L. Godet and S. F. Bent, *Adv. Funct. Mater.*, 2019, **29**, 1904129.

13 Y. Zhao and X. Sun, *ACS Energy Lett.*, 2018, **3**, 899–914.

14 L. Chen, Z. Huang, R. Shahbazian-Yassar, J. A. Libera, K. C. Klavetter, K. R. Zavadil and J. W. Elam, *ACS Appl. Mater. Interfaces*, 2018, **10**, 7043–7051.

15 L. Momtazi, H. H. Sønsteby, D. A. Dartt, J. R. Eidet and O. Nilsen, *RSC Adv.*, 2017, **7**, 20900–20907.

16 Z. Giedraityte, M. Tuomisto, M. Lastusaari and M. Karppinen, *ACS Appl. Mater. Interfaces*, 2018, **10**, 8845–8852.

17 A. I. Abdulagatov, K. N. Ashurbekova, K. N. Ashurbekova, R. R. Amashaev, M. Kh Rabadanov and I. M. Abdulagatov, *Russ. J. Appl. Chem.*, 2018, **91**, 305–318.

18 T. C. Bharat, Shubham, S. Mondal, H. S.Gupta, P. K. Singh and A. K. Das, *Mater. Today Proc.*, 2019, **11**, 767–775.

19 Y. Zhang, A. Apostoluk, B. Canut, S. Daniele and B. Masenelli, *Sci. Rep.*, 2019, **9**, 11959.

20 A. J. M. Mackus, J. R. Schneider, C. Macisaac, J. G. Baker and S. F. Bent, *Chem. Mater.*, 2019, **31**, 1142–1183.

21 M. Coll and M. Napari, *APL Mater.*, 2019, 7, 110901.

22 A. J. M. Mackus, C. Macisaac, W. H. Kim and S. F. Bent, *J. Chem. Phys.*, 2017, **146**, 52802.

23 C. Murray and S. D. Elliott, *ACS Appl. Mater. Interfaces*, 2013, **5**, 3704–3715.

24 J.-S. Na, Q. Peng, G. Scarel and G. N. Parsons, *Chem. Mater*, 2009, **21**, 5585.

25 J. W. Elam and S. M. George, *Chem. Mater.*, 2003, **15**, 1020–1028.

26 J. G. Baker, J. R. Schneider, J. A. Raiford, C. De Paula and S. F. Bent, *Chem. Mater.*, 2020, **32**, 1925–1936.

27 D. R. Zywotko and S. M. George, *Chem. Mater.*, 2017, **29**, 1183–1191.

28 C. Z. Leng and M. D. Losego, *Mater. Horizons*, 2017, 4, 747–771.

29 M. Li, X. Qian, A. D. Li, Y. Q. Cao, H. F. Zhai and D. Wu, *Thin Solid Films*, 2018, **646**, 126–131.

30 B. H. Lee, B. Yoon, A. I. Abdulagatov, R. A. Hall and S. M. George, *Adv. Funct. Mater.*, 2013, **23**, 532–546.

31 NIST X-ray Photoelectron Spectrosc. Database, NIST Stand. Ref. Database Number 20, Natl. Inst. Stand. Technol. Gaithersbg. MD, 20899.

32 E. Janocha and C. Pettenkofer, *Appl. Surf. Sci.*, 2011, **257**, 10031–10035.

33 D. Barreca, A. Milanov, R. A. Fischer, A. Devi and E. Tondello, *Surf. Sci. Spectra*, 2007, **14**, 34–40.

34 J. Duchoslav, R. Steinberger, M. Arndt and D. Stifter, *Corros. Sci.*, 2014, **82**, 356–361.